Iterative Metric-based Waveguide Optimisation

Lewis MacDonald	Celestion, Claydon Business Pk, Ipswich, IP6 0NL, England
Jack Oclee-Brown	KEF, Eccleston Rd, Maidstone, ME15 6QP, England
Mark Dodd	Celestion, Claydon Business Pk, Ipswich, IP6 0NL, England
Jonathan Hargreaves	University of Salford, The Crescent, Salford, M5 4WT, England

1 INTRODUCTION

In a recent paper, Dodd & Oclee-Brown[1] presented a novel approach to designing waveguides that are thin in one dimension. The technique uses corrugations and thickness variations to control how acoustic waves propagate. A subsequent paper[2] introduced two waveguide metrics which are computed from the solution to Laplace's equation. These metrics, the 'stretch' and 'felt area', respectively measure the relative path length and cross-sectional area change in a waveguide.

Together, they characterize a waveguide's ability to support single parameter (1P) wave propagation, which is where the pressure depends on only a single spatial coordinate and there is equal pressure magnitude across each entire wavefront[3]. When appropriately driven and terminated, waveguides which are good at supporting 1P wave propagation can transmit coherent waves without acoustic resonances or diffraction. The waveguide metrics are used to create a streamlined design approach for adding corrugations and thickness variations, and a waveguide modified using this technique demonstrated significantly improved wave coherence across a broad frequency range.

Building on this, this paper explores using the metric-based design procedure inside of an optimisation loop, further automating the process to achieve better acoustic performance. It then investigates the optimisation of a real-world design challenge - a line array wave-shaper and horn – comparing the optimised geometry to traditional designs. To test the technology, a sample is 3D printed and measured, and the measurements are compared to the simulation results. A larger sample with 120° horizontal and 60° vertical dispersion was also 3D printed and used in a listening test.

2 WAVEGUIDE METRIC EXAMPLES

This section demonstrates the waveguide metrics using basic geometric examples. The solution to Laplace's equation was computed using the FEA package PAFEC[6], and the resulting nodal data was then imported into MATLAB to calculate the waveguide metrics. For an in-depth explanation of the underlying mathematical theory and a detailed process of the metric calculation, refer to ref. 2.

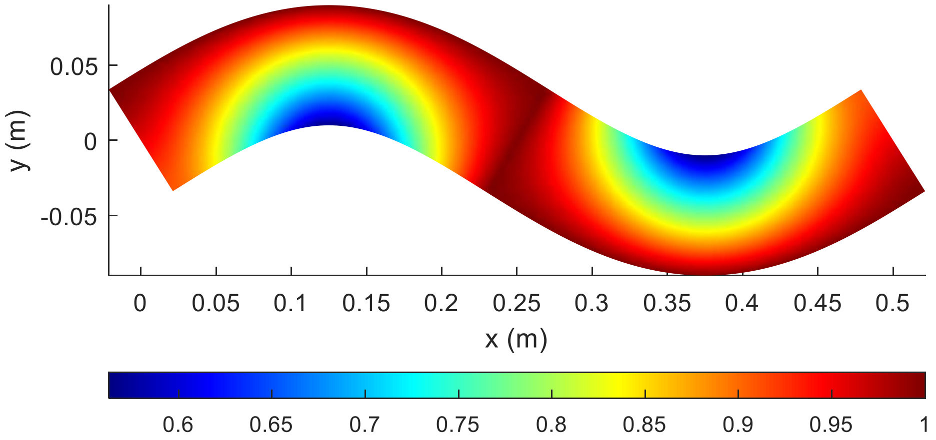

Figure 1: Normalised Stretch metric on a thickened sine curve

The Felt Area metric indicates how the relative cross-sectional area changes through a geometry, from entrance to exit. In Figure 2, the Felt Area metric illustrates that the cross-sectional area at the end of the wedge section is around three times as large than during the initial channel section (x=0).

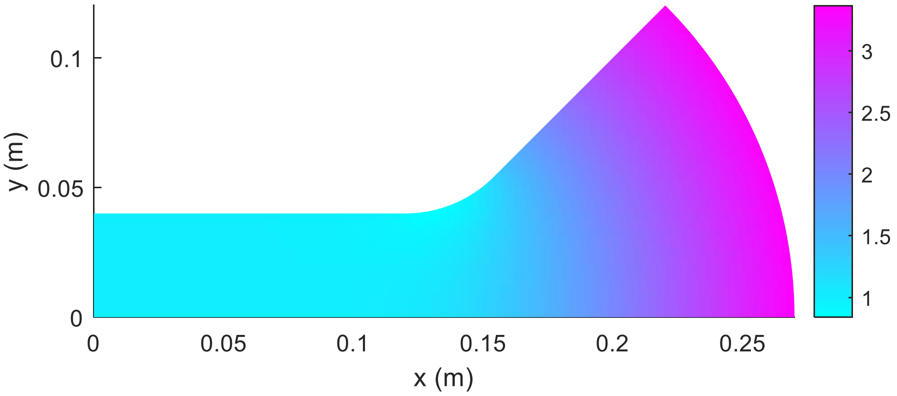

Figure 2:Felt Area metric on a channel-wedge geometry

Both waveguide metrics can be used to modify a geometry and make it better at supporting 1P wave propagation. This process reduces the error in the Stretch and Felt Area metrics respectively by equalizing the relative pathlength (through corrugations) and adjusting the domain thickness to obtain the desired area expansion[1,2].

3 ITERATIVE OPTIMISATION

Figure 3 outlines the optimisation loop process, in which the geometry undergoes iterative analysis and refinement.

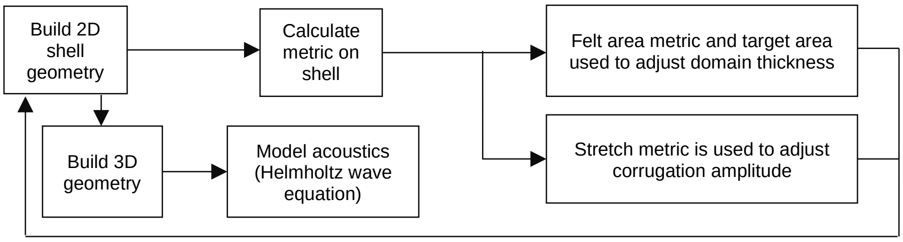

Figure 3: Iterative optimisation flow chart

By changing the material properties of the Laplacian FEA elements, it is possible to emulate varying thickness on a 2D shell mesh. This approach enables the area to be optimised while using just basic 2D shell elements, resulting in a very fast core optimisation loop.

To check the acoustic performance of the waveguide is also converging, the 2D mesh can be extruded into a 3D mesh to solve the Helmholtz wave equation. A constant velocity is used to excite the entrance surface and a suitable radiation boundary condition is used to terminate the domain.

Figure 4 shows the metrics during the optimisation of a simple in plane bend on iteration 1, 3, and 5. The initial flat geometry shows substantial error in both metrics, indicating that the design will be poor at supporting 1P wave propagation. On the subsequent iterations the error in each metric reduces. This is shown by the plot surface colour and the metrics MSE (mean square error) referenced to the first iteration.

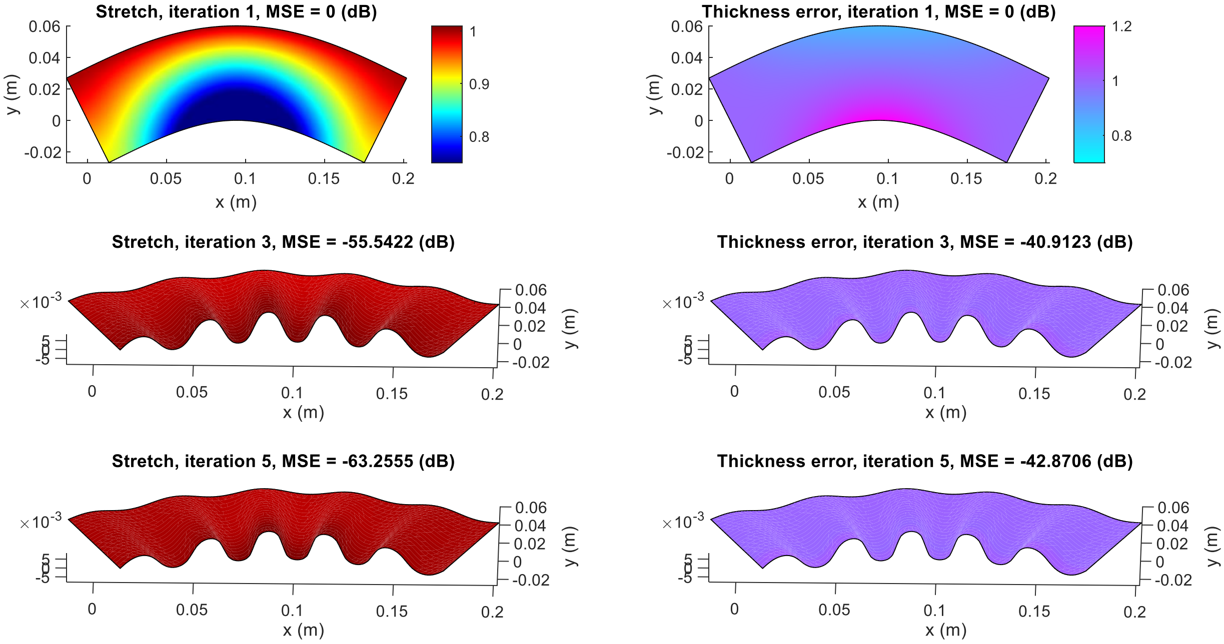

Figure 4: Stretch and thickness error on iterations 1, 3, and 5

Figure 5 presents the pressure distribution at 10kHz on iteration 1 and 5. The shell mesh has been extruded into 3D to allow an acoustic simulation. On the initial flat geometry, the pressure waves are reflected off the outside edge of the bend, leading to noticeably uneven wavefronts at the exit surface (around x=0.17). In contrast, on the optimised corrugated design (iteration 5), the pressure wavefronts are much more uniform throughout the geometry.

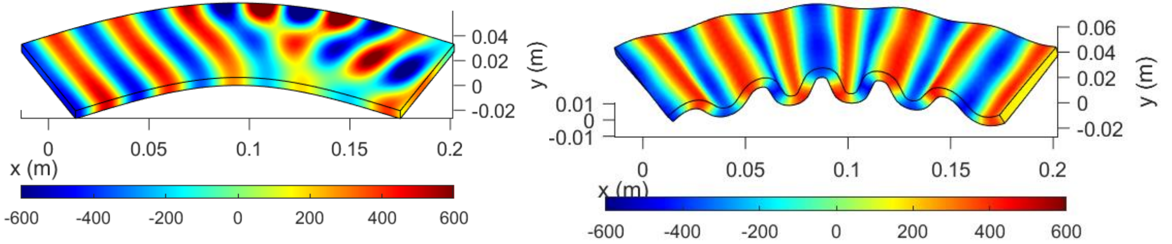

Figure 5: Pressure distribution at 10kHz, left: iteration 1, right: iteration 5

The maximum range in SPL across all the nodes on the exit surface was used to assess the acoustic performance over a broad range of frequencies. A perfectly uniform pressure wave at the exit would result in an SPL range of zero. Figure 6 shows the range of SPL over the exit surface of the example waveguide on iteration 1, 3 and 5.

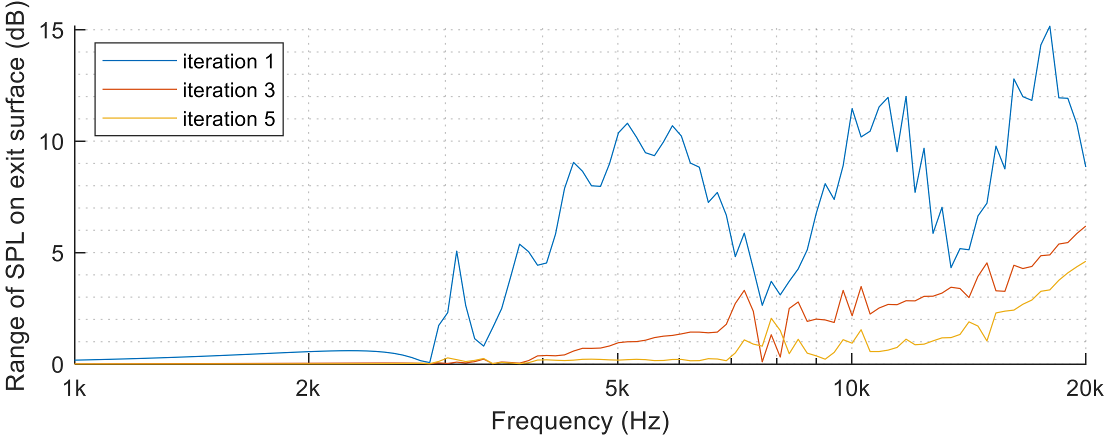

Figure 6:Range of SPL on exit surface: iteration 1, 3 and 5

On the first iteration, the large SPL range indicates that the pressure waves are highly disorganized over the exit surface. By iteration 3 a significant reduction in the range of SPL implies that the wavefronts have become more coherent over a wide range of frequencies. As the optimisation process continues to iteration 5 the range in SPL is further minimized, however the changes in the geometry are more subtle (see Figure 4). These results show a correlation between the acoustic performance of the waveguide and the waveguide metrics shown in Figure 4.

4 LINE ARRAYS

Most line arrays use a "wave-shaper" to convert the circular shape plane wave produced by a compression driver into the thin rectangular plane wave required at the horn mouth of the line array. There are many contrasting design approaches found in commercial line array wave-shapers[4,5].

Line arrays typically have a horn section in front of the wave-shaper that helps control the directivity and/or throat impedance. The design of these horns involves a trade-off between achieving good throat impedance (exponential expansion), or wider and more constant directivity but with poorer throat impedance (conical diffraction style horn). The throat impedance is the load which is applied to the driver. Although somewhat reduced in magnitude, ripples found in the throat impedance will also be observed in the frequency response of the radiated sound pressure level from the combined horn -driver system.

5 NOVEL WAVE-SHAPER AND HORN

The method outlined in section 2 was used to develop a line array wave-shaper and horn.
Each part was optimised separately (around 8 iterations) and uses the pathlength equalisation corrugations and thickness adjustment technology to control the propagating sound waves.

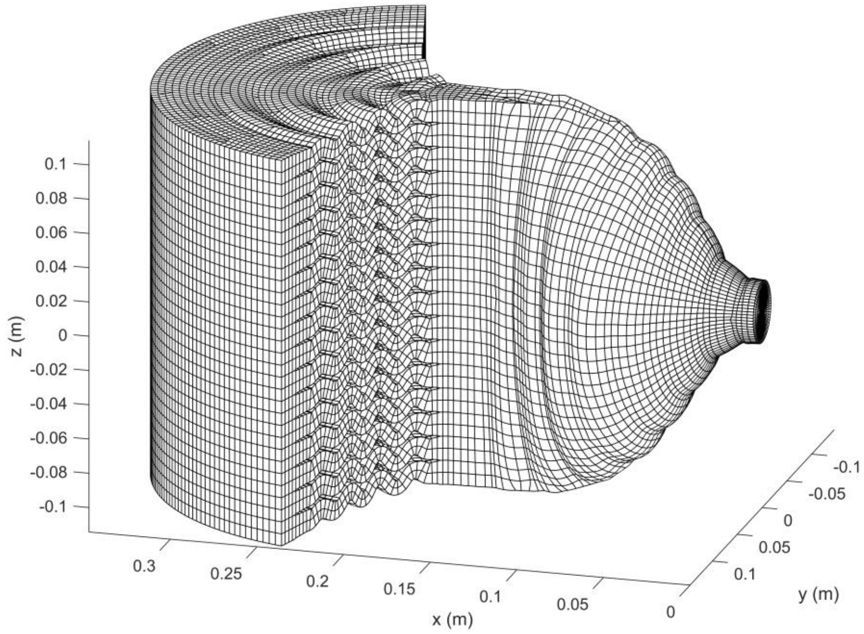

Figure 7: FEA mesh of example 150° optimised wave-shaper and horn

Figure 7 shows the FEA mesh of the air in the assembly. The initial wave-shaper section converts the circular plane waves from the compression driver into rectangular plane waves (around x = 0.15). Corrugated "fins" are then used to divide the horn into 16 channels which help control the throat impedance and convert the rectangular plane waves into 150° cylindrical waves. The design achieves very wide constant directivity whilst having controlled throat impedance - something that is hard to achieve with traditional horn design techniques. The same design approach can be used to create many intriguing wavefront shapes suitable for a variety of diverse applications.

6 ASSEMBLY RESULTS

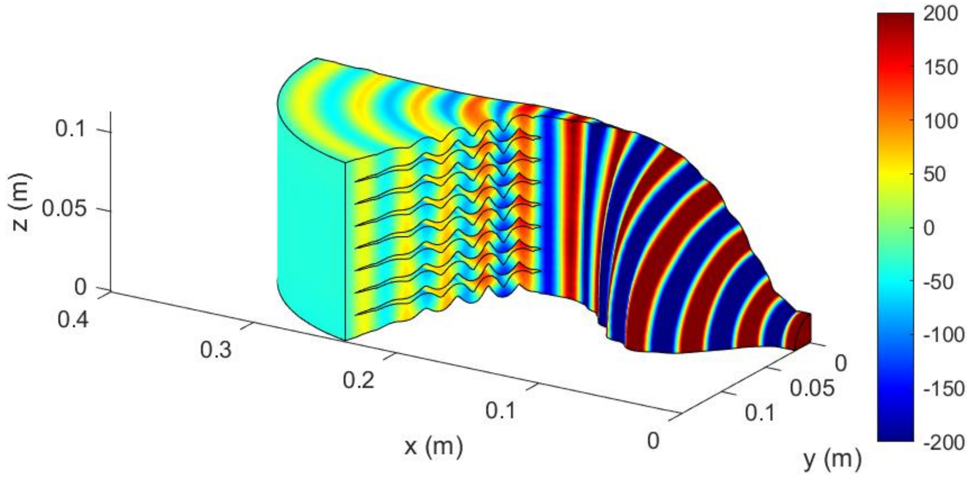

Figure 8: Pressure distribution at 10kHz on example optimised line array wave-shaper and horn assembly

Figure 8 is the FEA simulated pressure distribution inside an optimised line array wave-shaper coupled to an optimised 150° horn. Due to the device's symmetry in two planes only a quarter of it is modelled. The simulation illustrates how the pressure waves evolve through the different sections of the assembly, starting with circular plane waves (x=0), then rectangular plane waves (x=0.15), and finally cylindrical shaped waves on the exit surface.

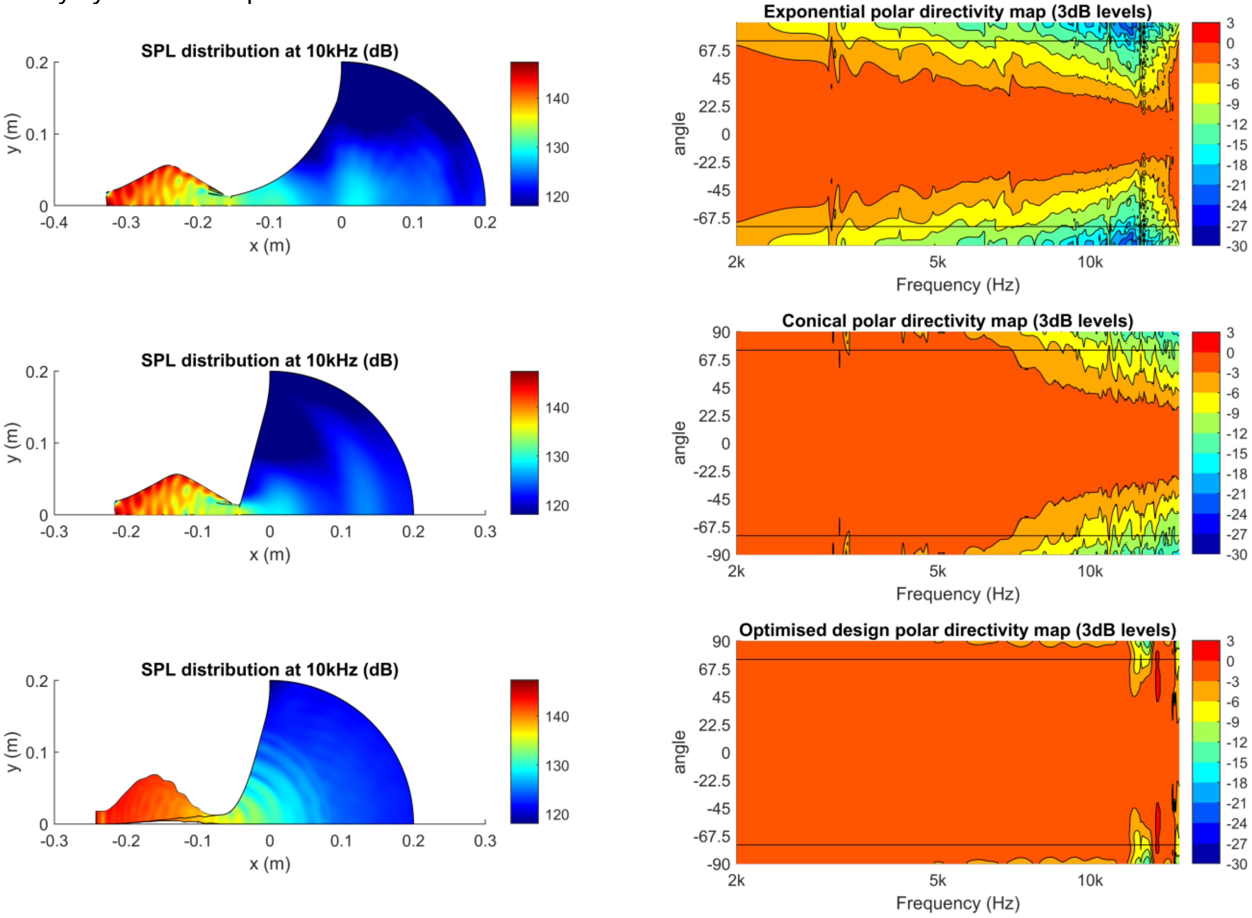

Figure 9: Comparison of example wave-shaper with exponential horn, example wave-shaper with conical horn, and an optimised wave-shaper and optimised horn. Left: SPL at 10kHz, Right: normalized horizontal directivity

Figure 9 compares the horizontal directivity of three line array horn and wave-shaper configurations:

1. Example wave-shaper with an exponential horn
2. Example wave-shaper with a conical diffraction style horn
3. Optimised wave-shaper with an optimised horn

All configurations share the same final horn section which is angled at 150° and then curves around to a flat baffle. Black lines mark the +/-75° point on the directivity maps. PAFEC FEA was used to simulate the Helmholtz wave equation. The domain was excited with a constant velocity over the entrance surface (left side) and terminated with a cylindrical radiation boundary on the exit.

Compared to the exponential horn, the conical-diffraction horn has wider directivity up to a higher frequency, which explains its common use in commercial line array systems. The broader dispersion at high frequencies is achieved through a narrow throat and sudden change in area expansion, however this can cause problems with the throat impedance.

The optimised corrugated line array horn is designed to emit cylindrical wavefronts so it has consistently wide directivity up to around 13kHz, at which point it starts to narrow slightly. The area expansion is also controlled in each section to improve the throat impedance.

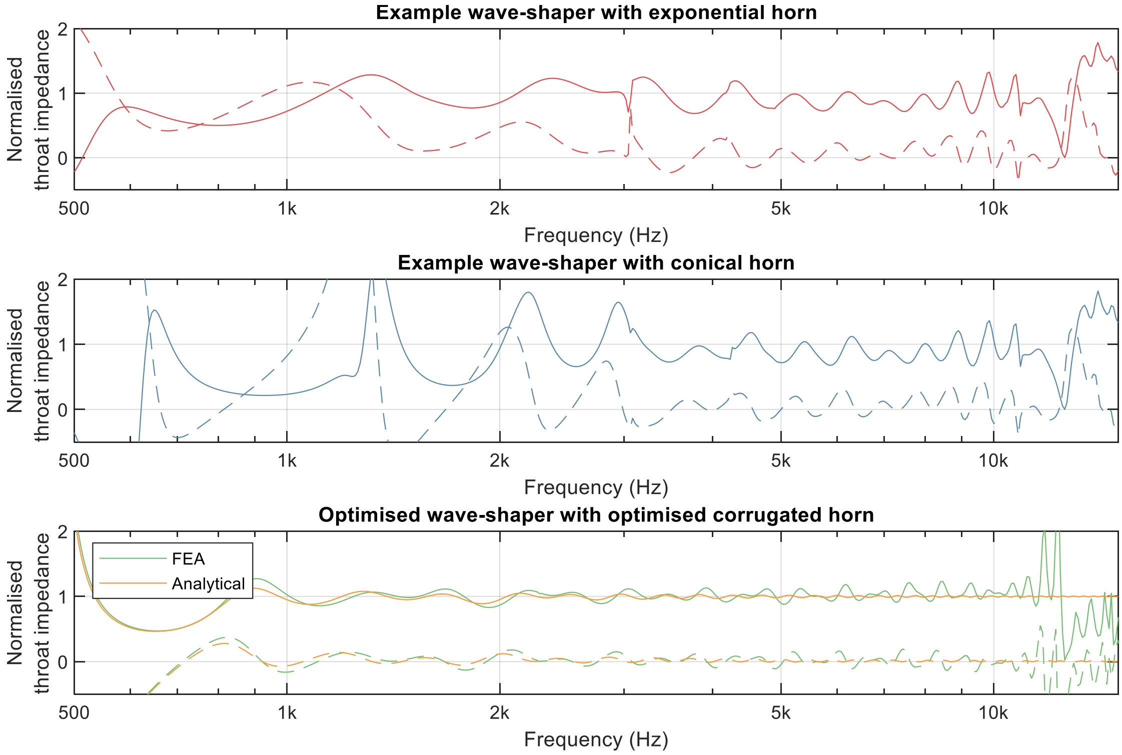

Figure 10: Normalized throat impedance of line array assemblies (Solid Line: real, Dashed Line: imaginary).

Figure 10 compares the throat impedance from each of the designs shown in Figure 9. On the conical horn model, the abrupt change in area expansion at the transition between the wave-shaper and the wide 150° conical horn causes strong reflections to the propagating sound waves, resulting in large ripples in the throat impedance. The smaller ripples in the exponential horn model are due to a less severe impedance mismatch between the wave-shaper (f_c=195Hz) and the exponential horn (f_c=450Hz), and at the exit of the exponential horn and the flat baffle.

The optimised horn and wave-shaper have less significant impedance ripples due to the tuning of the area expansion inside each section. The relatively small ripples and the dip around 600hz are due to how at the end of the corrugated 'fins', as the material disappears, the area expands faster than if it was in a simple conical horn. Adjusting the fin dimensions can shift the dip's frequency.

The 1D analytical throat impedance is also included for the optimised design. A waveguide which is good at supporting 1P wave propagation can be modelled unusually accurately using a 1D lumped parameter model. Below 10kHz the differences in these results are due to how the corrugated fins in the FEA model have been truncated at each end when the thickness is less than 1mm. The high frequency differences arise due to reflections of the soundwaves inside of the corrugations.

7 PHYSICAL MEASUREMENTS

For validation, a similar 150° optimised line array wave-shaper and horn designed for a Celestion CDX1425 compression driver was 3D printed and measured in a large waveguide capable of supporting cylindrical wave radiation (see Figure 11). The measurement waveguide replicates the acoustic load on the horn that would be found in an infinite vertical array and includes microphone positions for measuring the horizontal directivity. The measurement was time windowed to remove unwanted reflections from the end of the waveguide.

Figure 11: Measurement set up photos. Left: 3D printed optimised wave-shaper and horn, Right: Measurement waveguide with microphone positioned on axis

Figure 12 presents the normalised directivity measurements alongside the normalised directivity simulation. The directivity maps use 1dB increments to reveal the fine details in the directivity pattern. The waveguide achieves very wide directivity across a broad frequency range, and there is a good match between the simulation and measurement.

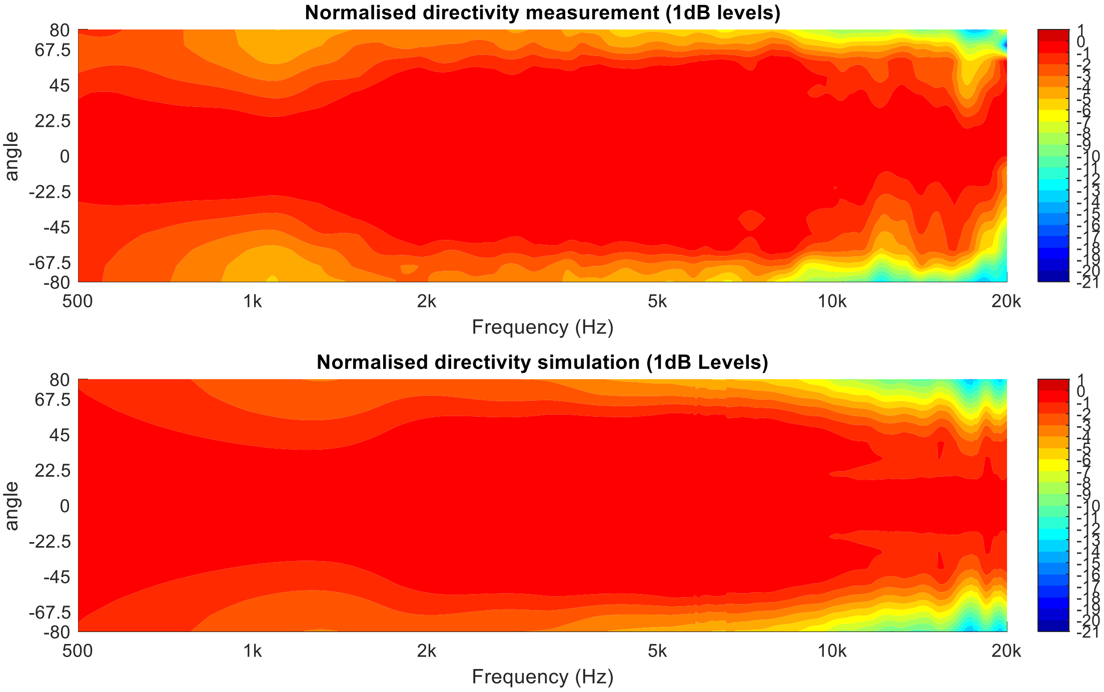

Figure 12: Horizontal directivity. Top: Measurement, Bottom: Simulation

8 LISTENING TEST

A toroidal line array source with 60°x120° coverage, combining the output of four 1-inch exit compression drivers into a single source (Figure 13), was built and showcased in a system during the Celestion 100-year anniversary open day. The listening demonstration received highly positive feedback and gives an example of a practical implementation using the methods described here.

9 DISCUSSION AND CONCLUSIONS

The waveguide optimisation process in Figure 4 equalizes the relative pathlength and area expansion within a geometry, reducing the error in the corresponding metrics. This improves the geometry's ability to support coherent wave propagation. The optimised line array assembly from section 5 and 6 also achieves neat, aligned, wavefronts over a wide frequency range.

Above 12kHz the optimised model shows some irregularities in the throat impedance and reduced directivity control. This is due to the channel thickness becoming significant in comparison to the wavelength at high frequencies, at which point the sound waves begin to reflect off the corrugation surfaces. The extent of this depends on the amplitude and periodic length of the corrugations in relation to the acoustic wavelength. To improve the performance at higher frequencies, the air channels can be made thinner.

Investigating the differences in far-field SPL between coherent and less coherent line array sources would be interesting. The work could also be extended to include modelling the behaviour of the termination flare.

The metrics in ref. 2 were applied to two "thin waveguide" concepts in ref. 7 using an optimisation loop. The convergence of the metrics is strongly associated with an improved acoustic performance over a useful frequency range. The iterative process allows rapid evaluation and improvement of a line array wave-shaper and horn. While this approach adds complexity, it allows the directivity, acoustic impedance, and coherence to all be simultaneously optimised meaning many new design options can be explored, such as waveguides that produce wavefront shapes for arraying, focusing, and combining acoustic sources in ways which were not previously possible.

Figure 13: 60°x120° Source with 4 1-inch compression drivers. Top: photo, Bottom: CAD section view

10 REFERENCES

1. M. Dodd and J. Oclee-Brown, 'Wave-shaping using novel single-parameter waveguides', presented at the Audio Engineering Society Convention 153, Oct. 2022.
2. L. MacDonald, J. Oclee-Brown, and J. Hargreaves, "Metric based development of acoustic lenses and waveguides," Institute of Acoustics, vol. 44, pt. 3, 2022.
3. G. R. Putland, "Every one-parameter acoustic field obeys Webster's horn equation," J. Audio Eng. Soc., vol. 41, no. 6, (1993).
4. J. Spillmann and S. Riemersma, "Acoustic waveguide," U.S. Patent 9,571,923 B2, Feb. 14, 2017.
5. C. Heil, "Sound wave guide," U.S. Patent 5,163,167 A, Nov. 10, 1992.
6. PACSYS Ltd., PAFEC-FE. PACSYS Ltd., 2008.
7. M. Dodd and J. Oclee-Brown, "Acoustic waveguides," European Patent GB2588142, EP3806086A1, 2020.